INNOVATIVE TOOLS FOR SCIENTIFIC COMPUTATION
IN AERONAUTICAL ENGINEERING
J. Periaux, P. Joly, O. Pironneau and E. Oñate (Eds.)

A SIMPLE METHOD FOR AUTOMATIC ADAPTION OF FINITE ELEMENT MESHES TO CHANGES IN THE BOUNDARY SHAPE

Giorgio Chiandussi
Department of Mechanical Engineering
Technical University of Turin
Corso Duca degli Abruzzi 24
10129 Torino, Italy
Email: chindussi@polito.it
web page:http://www.polito.it

Gabriel Bugeda and Eugenio Oñate
International Center for Numerical
Methods in Engineering (CIMNE)
Universidad Politécnica de Cataluña
C/ Gran Capitán s/n; Campus Norte UPC; C1
08034 Barcelona, Spain
Email:bugeda@cimne.upc.es
web page: http:/www.cimne.upc.ei

Abstract. A simple method to automatically update the finite element mesh of the analysis domain is proposed for cases when the shape of the domain is modified. The method considers the mesh as a fictitious elastic body subjected to prescribed displacements at selected boundary points. The mechanical properties of each mesh element are appropriately selected in order to minimise the deformation and the distortion of the mesh elements. Different selection strategies have been used and compared in their application to simple examples. The method avoids the use of remeshing in the solution of shape optimisation problems and reduces the number of remeshing steps in the solution of coupled fluid-structure interaction problems.

Key words: automatic mesh update; shape optimisation; fluid-dynamic analysis; aerodynamic analysis; finite element method.

1 INTRODUCTION

Two extremely different computational problems such as shape optimisation and fluid-structure interaction analysis are characterised by a common requirement concerning geometrical changes in the boundary shape. In shape optimisation problems the surfaces defining the boundaries of a structure need to be continuously modified during the search for an optimal solution[1,3,4,5]. Also, during the solution of a coupled fluid-structure interaction problem, the position of an object immersed in the fluid needs to be continuously updated according to the values of the interacting forces[2]. In this case, the complexity of the problem can be increased by the presence of a free surface.
The modification of a surface of an object as well as the change of position of a body inside a fluid requires the modification of the mesh used for the computations. The mesh update step can be achieved by using a remeshing process. The final result would be valid providing the geometric model of the structure is updated prior to the remeshing step by using data obtained in previous analyses, which is usually difficult in

practice. Moreover, in shape optimisation problems the use of different meshes can introduce a significant amount of numerical noise that makes difficult the convergence towards the optimal solution. It is then of the utmost interest to identify a method able to reduce the need of remeshing.

Different mesh moving strategies have been proposed in recent years, mostly connected with fluid-structure interaction problems. A powerful and commonly used approach is to view the mesh as a pseudo-structural system. This could be done through a spring/mass type idealisation[6,9] or by solving directly the elasticity equations[7,8]. The crucial point of this type of methods is how to select the stiffness of the pseudo-structural elements in order to achieve a mesh with the desired properties. Typical choices are based on simple distance criteria, which are computationally effective but can lead to high distortion in the mesh elements in the presence of large movements.

In this paper a simple method to update the mesh leading to a minimum element distortion is presented. The method is based on the pseudo-structural approach; i.e., the mesh is considered as an elastic body subjected to prescribed motions on its boundaries. The elastic properties of each element are appropriately selected so as to ensure minimum element distortion during the mesh movement. The application of the proposed technique eliminates the need of remeshing in shape optimisation problems where surface displacements are moderate. In fluid-dynamic problems where the position of the structure can change significantly the use of the remeshing techniques can be reduced; the advantages offered by the proposed technique can be limited by the need to redefine the boundary conditions at the fluid-structure interface.

The content of this chapter is structured as follows. In the next section the basic ideas behind the proposed mesh moving procedure are presented. The different alternatives studied for the material property selection in the fictitious structural model are then discussed. The different procedures are compared through the analysis of a mesh movement problem due to the change of position of an airfoil within a 2D fluid domain. Some conclusions on the best moving algorithms found are finally drawn.

2. THE METHOD

Every structure is identified by its geometrical boundaries. A modification of the shape as well as the change of position of the structure can be seen, at a discrete model level, as a displacement of the nodes belonging to the boundaries of the finite element mesh. Given the displacements of the boundaries, their influence on the position of the mesh internal nodes can be taken into account by considering the mesh as a fictitious structure. By solving a linear structural problem with the displacements of the moving surfaces as prescribed displacements, it is possible to obtain the displacements of the mesh nodes. If a fluid-dynamic problem is analysed, it is necessary to ensure that the surfaces that limit the control volume containing the fluid remain fixed in the solution of the pseudo-structural problem.

Unfortunately the solution of the structural problem by considering the mesh formed by an isotropic and homogeneous linear material introduces a high element distortion during the mesh updating process. Typically, elements close to the changing surfaces are constrained to modify their shape much more than those elements located far from these surfaces. This behaviour frequently leads to extremely distorted meshes near the boundaries and, in the limit, to not conforming meshes and intersecting elements.

Note that finite elements in the mesh are used in this process as an interpolation method and, consequently, the stresses obtained in the pseudo-structural problem are not relevant. This allows to select and to assign different mechanical properties to each

mesh element. In this way, it is possible to distribute the mesh deformation more uniformly all over the elements by assigning stiffer material properties to the elements near the moving surfaces. Different constitutive laws can be adopted following geometrical or physical criteria. For example, following a pure geometrical criterion, the Young modulus of each mesh element can be selected depending on its minimum distance to the closest changing surface. Alternatively, the Young modulus can be selected depending on the element strains or the element strain energy density obtained from a previous analysis using uniform material properties. The different alternatives for the material properties selection studied in this work are described in the next sections.

2.1 Selection of material properties based on a geometric criterion

The selection of the element material properties (namely, the Young modulus) is here based on a pure geometrical criterion. The Poisson ratio can be chosen independently. Once the barycentre $\bar{\mathbf{x}}_b$ of an element has been found, it is possible to evaluate its distance d to the nearest node $\mathbf{x}$ belonging to a moving surface by:

$$d = \sqrt{(x_{1b} - x_1)^2 + (x_{2b} - x_2)^2 + (x_{3b} - x_3)^2} \tag{1}$$

Three different strategies have been considered with the Young modulus distribution law depending on d as follows:

$$\text{Linear law } (E \propto d) \tag{2}$$

$$\text{Quadratic law } (E \propto d^2) \tag{3}$$

$$\text{Exponential law } (E \propto e^d) \tag{4}$$

2.2 Selection of material properties based on a previous analysis

In this case, the mesh update problem is performed in two steps. In the first step the discrete model is assimilated to a structural model characterised by an isotropic homogeneous material with Young modulus $\bar{E}$. A fictitious linear structural problem is then solved by imposing prescribed displacements corresponding to the known surface movements. The strain field computed in the first step is used in the second step to evaluate the new Young modulus for the different mesh elements using one of the strategies described in the next subsections. The pseudo-structural mesh with the new material properties (in principle, a different material property for each element) is analysed once more. The solution of this second pseudo-structural problem yields the correct displacement of the mesh nodes ensuring quasi-uniform element distortion.

The quality of the deformed mesh is assessed by controlling the element aspect ratio and preventing that no side intersection occurs. A straightforward, although expensive, check can be based in verifying the sign of the determinant of the element jacobian. A simpler rule can be based in checking the angles between the consecutive element sides of each element.

2.2.1 Selection of material properties based on the element strain field.

Let us consider a one-dimensional bar. The result of a linear analysis with arbitrary prescribed displacements at several bar points and a homogeneous material with Young

modulus $\bar{E}$ allows to compute the stress and strain fields over the bar. In this case, a non-uniform strain distribution would be obtained. Stress and strain are related by the well-known relationship:

$$\sigma = \bar{E}\varepsilon \tag{5}$$

If a constant strain field $\bar{\varepsilon}$ is required with the same stress distribution σ, it is necessary to allow the Young modulus to change in a continuous way over the bar. The relationship between the stress σ and the constant strain field $\bar{\varepsilon}$ is:

$$\sigma = E\bar{\varepsilon} \tag{6}$$

Assuming the same stress field for both cases, it is possible to use expressions (5-6) to obtain the value of the continuous Young modulus to be assigned at each point of the bar as:

$$E = \frac{\bar{E}}{\bar{\varepsilon}}\varepsilon \tag{7}$$

Equation (7) allows obtaining a solution with the same stress distribution than the original one but with a constant strain distribution. The Young modulus is proportional to the strain value and the proportionality coefficient is defined by the ratio between the Young modulus used in the first analysis $\bar{E}$ and the sought constant strain field $\bar{\varepsilon}$. The initial Young modulus $\bar{E}$ can be chosen, for example, equal to a unit value. In this case the proportionality coefficient is simply the inverse of the sought constant strain field.

In case of a finite element discretization, expression (7) allows to obtain a new value for the Young modulus for each mesh element. Using these new values, a second finite element analysis would provide a uniform strain field.

The same method can be adopted for two as well as three-dimensional (3D) structures. Starting from a linear analysis with an isotropic homogeneous material with Young modulus $\bar{E}$, the principal stresses for a 3D problem can be evaluated in terms of the principal strains as:

$$\sigma_i = \frac{E(1-\nu)}{(1+\nu)(1-2\nu)}\varepsilon_i + \frac{\nu}{1-\nu}(\varepsilon_j + \varepsilon_k), \quad i,j,k = 1,3 \quad i \neq j \neq k \tag{8}$$

If an imposed constant strain field ($\bar{\varepsilon}_1 = \bar{\varepsilon}_2 = \bar{\varepsilon}_3 = \bar{\varepsilon}$) and an orthotropic linear elastic material are considered, stresses are then given by:

$$\sigma_i = \frac{E}{(1-2\nu)}\bar{\varepsilon}, \quad i = 1,3 \tag{9}$$

If the same stress field is required to exist in both solutions, the following equations need to be satisfied:

$$E_i = \frac{E(1-\nu)}{\varepsilon(1+\nu)}\varepsilon_i + \frac{\nu}{1-\nu}(\varepsilon_j + \varepsilon_k) \quad i,j,k = 1,3 \quad i \neq j \neq k \tag{10}$$

In this case the method would require the selection of as many anisotropic materials as the number of elements. This process would require the storage of the stiffness matrix of each element. If a Poisson ratio $\nu = 0$ is considered, expression (10) can be simplified as follows:

$$E_i = \frac{\bar{E}}{\bar{\varepsilon}}\varepsilon_i \quad i = 1,3 \tag{11}$$

The Young modulus in each principal direction depends only on the corresponding principal strain. An approximate simpler solution that has also been tested which is independent of the Poisson ratio value consist in choosing the Young modulus to be assigned to each mesh element as the mean value of the expressions (11):

$$E = \frac{\bar{E}}{\bar{\varepsilon}}\sqrt{\frac{\varepsilon_1^2 + \varepsilon_2^2 + \varepsilon_3^2}{3}} \tag{12}$$

Also, the following expression based on the square mean value of strains has been tested:

$$E = \frac{\bar{E}}{\bar{\varepsilon}^2}\frac{\varepsilon_1^2 + \varepsilon_2^2 + \varepsilon_3^2}{3} \tag{13}$$

2.2.2 Selection of material properties based on the element strain energy density

A strategy based on the element strain energy density has also been considered. By evaluating the principal strains and stresses, the strain energy density of every mesh element after the first linear structural analysis is computed by:

$$U = \frac{1}{2}(\sigma_1\varepsilon_1 + \sigma_2\varepsilon_2 + \sigma_3\varepsilon_3) \tag{14}$$

Substituting equation (8) into (14), it is possible to express the strain energy in terms of $\bar{E}$ and the principal strain field. Now, in order to obtain a new solution with a uniform strain energy density, the new Young modulus to be assigned to the mesh elements for the second analysis can be made proportional to the strain energy density:

$$E = \frac{E(1-\nu)}{2(1-2\nu)(1+\nu)}(\varepsilon_1^2 + \varepsilon_2^2 + \varepsilon_3^2) + \frac{2\nu}{1-\nu}(\varepsilon_1\varepsilon_2 + \varepsilon_2\varepsilon_3 + \varepsilon_3\varepsilon_1) \tag{15}$$

In this case the Young modulus for each element depends on the arbitrary Young modulus E and the strain field of the element evaluated in the principal strain reference system.

2.2.3 Selection of material properties based on the distortion energy density

Another strategy based on the evaluation of the distortion energy density of the elements has been tested. By evaluating the principal strains and stresses, the distortion energy density of every mesh element after the first linear structural analysis is computed by:

$$U_d = \frac{\overline{E}}{12(1+\nu)}\left[(\varepsilon_1-\varepsilon_2)^2+(\varepsilon_2-\varepsilon_3)^2+(\varepsilon_3-\varepsilon_1)^2\right] \tag{16}$$

In this strategy, the new Young modulus for each element of the mesh used for the second analysis is proportional to the distortion energ, i.e.:

$$E = \frac{\overline{E}}{12(1+\nu)}\left[(\varepsilon_1-\varepsilon_2)^2+(\varepsilon_2-\varepsilon_3)^2+(\varepsilon_3-\varepsilon_1)^2\right] \tag{17}$$

3. EXAMPLES

The strategies above identified and explained have been applied to a two-dimensional problem concerning the change of position of an airfoil inside a fluid domain meshed using triangular 3 nodded elements. Two cases have been analysed: 1) the vertical displacement of the trailing edge of the airfoil and 2) the vertical change of position of the entire airfoil (see Figure 1). The first case corresponds, for small displacements, to a rotation of the airfoil around the leading edge. The strategies for selecting the non-uniform Young modulus for every mesh element are summarised in Table 1.

The first strategy is based on a constant Young modulus distribution that can be selected arbitrarily. The Young modulus distribution obtained with the other strategies has been constrained to the range 1-100 N/mm^2. The quality of the deformed meshes provided by each proposed strategy has been measured by using the following mesh quality indicator (MQI):

$$MQI = \sqrt{\frac{1}{3 * \text{elements}_{\text{elements}}}\sum_{i=1}^{3}(60^\circ-\theta_i)^2} \tag{18}$$

Strategy 1	Isotropic homogeneous material with arbitrary Young modulus.
Strategy 2	Young modulus proportional to the distance of the element to the nearest modified surface (expression (2)).
Strategy 3	Young modulus varying exponentially in terms of the distance of the element to the nearest modified surface (expression (4)).
Strategy 4	Young modulus proportional to the square of the distance of the element to the nearest modified surface (expression (3)).
Strategy 5	Young modulus depending on the norm of the element principal strains (expression (12)).
Strategy 6	Young modulus depending on the element strain energy density (expression (15)).
Strategy 7	Young modulus depending on the element distortion energy density (expression (17)).
Strategy 8	Young modulus depending on the square norm of the element principal strains (expression (13)).

Table 1: Strategies for the selection of the Young modulus.

	1	2	3	4	5	6	7	8
example 1	18%	21%	32%	55%	51%	84%	88%	87%
example 2	24%	29%	53%	79%	89%	85%	77%	81%

Table 2: Maximum vertical displacement of the airfoil trailing edge and of the entire airfoil expressed in percentage of the chord length for each strategy.

where θ_i is the angle at each corner of each element triangle measured in sexagesimal degrees. Also the minimum and the maximum angle present in the mesh have been considered for a comparison. The MQI measures how uniform is the deformation over the mesh elements, whereas the minimum and maximum angles allow to identify how much deformed is the most critical element in the same mesh. The MQI of eq. (18) alone is not sufficient to identify the best strategy to adopt because it is scarcely influenced by the presence of little areas containing highly distorted elements as it happens in the leading and the trailing edges of the airfoil for the considered example. Conversely, these areas with highly deformed elements can also be identified using a simpler indicator such as the maximum and the minimum angles of the elements.

Different numerical experiments performed by using four different Poisson ratios have shown that a Poisson ratio of $\nu = 0.32$ provides the best results for all strategies. Due to that reason, the following results for the different strategies were obtained with this value of the Poisson ratio.

The configurations corresponding to the maximum vertical displacement of the airfoil trailing edge (first example) and to the maximum vertical displacement of the entire airfoil (second example) without element intersection have been identified for the eight strategies above described. The maximum displacement values for these configurations have been evaluated with reference to the airfoil chord. The results obtained are summarised in Table 2.

It is necessary to remember that in the first example the maximum displacement achievable by the airfoil before reaching the fluid domain boundaries is only the 94% of its chord due to its thickness.

For each strategy, the quality parameters defined above have been evaluated in correspondence of two reference displacements. These reference displacements have been defined as:

The maximum displacement achieved with the strategy based on a uniform Young modulus distribution law (strategy 1)

A 50% chord length displacement of the airfoil.

The first reference displacement allows to compare the results obtained with the first strategy and those obtained with the other ones. The second reference displacement allows to compare between the best strategies analysed. In this way, it is possible to verify the differences in the mesh quality obtained with large displacements of the airfoil for the different strategies.

Table 3 summarises the results obtained by using the first example concerning the airfoil rotation. They have been evaluated for a vertical displacement of the trailing airfoil edge equal to the maximum allowable obtained with strategy 1 (18% of the airfoil chord length) and for a 50% reference vertical displacement. The values of the quality parameters for the starting mesh are shown in the first column.

The quality parameters for the second example concerning the airfoil vertical displacement are shown in Table 4. They have been evaluated for a vertical displacement of the airfoil equal to the maximum allowable obtained with strategy 1

(24% of the airfoil chord length) and for a 50% reference vertical displacement. The

			strategy							
		initial	1	2	3	4	5	6	7	8
18% airfoil chord length reference displacement	θ_{max}	105.0	169.3	133.4	119.6	113.7	110.8	107.3	107.5	106.6
	θ_{min}	30.4	1.9	5.9	14.6	27.7	27.4	27.1	27.0	27.3
	MQI	8.7	10.9	10.6	10.0	10.5	10.1	10.1	10.1	9.9
50% airfoil chord length reference displacement	θ_{max}	105.0	--	--	--	164.5	172.7	136.8	134.6	135.2
	θ_{min}	30.4	--	--	--	4.7	18.9	14.4	15.3	15.0
	MQI	8.7	--	--	--	18.9	17.0	17.0	16.9	16.9

Table 3: Values of the maximum angle, the minimum angle and the mesh quality indicator MQI for the initial and the deformed meshes of the airfoil trailing edge vertical displacement. Data have been evaluated by using all strategies and with the 18% and 50% airfoil chord length references.

values of the quality parameters for the starting mesh are shown in the first column.

The results represented in Tables 2, 3 and 4 allow to extract the following conclusion:

Strategies 2 and 3, respectively based on the linear and quadratic variation of the Young modulus, produce a slight improvement with respect to strategy 1. Nevertheless, this improvement is not large enough to allow for a 50% airfoil chord length movement.

Strategy 4 is the best of all strategies based on geometrical criteria. It allows for a 50% airfoil chord length movement, but it is not as good as strategies 6, 7 or 8.

Strategy 5 is not better than strategy 4.

Strategies 6, 7 and 8 provide results that are significantly better than the rest. The differences between these three strategies are small in comparison with the improvements they produce in comparison with the rest.

The strategy based on an isotropic homogeneous material (strategy 1) leads to a strong deformation of the elements near the airfoil boundaries. The maximum displacement the airfoil can be subjected to is very small. In Figure 1 the original NACA0012 mesh is shown (first row). The second and third rows show the trailing edge vertical displacement and the vertical position change including a general view of the mesh and a detail of the most distorted elements. The maximum trailing edge vertical displacement before element intersection found is about 18% of the chord length (second row). The maximum vertical displacement of the airfoil before element intersection found is about 24% of the chord length (third row).

The maximum displacements obtained by using strategy 1 (second row), and the 50% chord length displacement have been taken as reference displacements for comparison with results obtained with the different strategies. The maximum displacement that can be obtained with each strategy will be shown in the fourth row of each figure.

Comparing the geometrical criteria (strategies (2-4)), the criterion based on the square of the distance of each element to the nearest modified surface (strategy 4) showed the best results. The results obtained using this strategy,are shown in Figures 2-3. Note the uniformity of the mesh compared to the solution obtained using an isotropic homogenous material (Figure 1). This strategy is very effective in the second example concerning the airfoil vertical displacement whereas some difficulties due to the

presence of a highly deformed area around the trailing edge of the airfoil are shown in the first one.

The strategy based on the evaluation of the norm of the principal strains of each element (strategy 5) shows an extremely different behaviour in the two examples analysed. In the second one it behaves very well, whereas in the first example it shows a worse performance.

The results obtained with strategy 6 based on the element strain energy density are shown in Figures 4-5. The results obtained with strategy 7 based on the element distortion energy density and the ones obtained with strategy 8 based on the square of the strain vector norm are shown in Figures 6-7 and Figures 8-9 respectively. Globally, these last three strategies have provided the best results in the two examples analysed with very small differences between them. They can be considered as the most efficient.

			strategy							
		initial	1	2	3	4	5	6	7	8
18% airfoil chord length reference displacement	θ_{max}	105.0	177.8	167.9	143.8	116.7	125.2	112.6	112.0	111.9
	θ_{min}	30.4	0.6	4.6	16.2	23.3	25.1	25.0	23.9	24.4
	MQI	8.7	14.9	13.9	12.2	13.7	13.2	13.0	12.9	12.9
50% airfoil chord length reference displacement	θ_{max}	105.0	--	--	--	148.9	154.7	134.9	133.3	133.6
	θ_{min}	30.4	--	--	--	12.4	10.1	15.0	12.7	13.8
	MQI	8.7	--	--	--	23.5	22.7	22.1	22.2	22.1

Table 4: Values of the maximum angle, the minimum angle and the mesh quality indicator MQI for the initial and the deformed meshes of the airfoil vertical displacement. Data have been evaluated by using all strategies and with the 24% and 50% airfoil chord length references.

4. CONCLUSIONS

The proposed method for mesh updating can be used to eliminate the need of remeshing in the solution of shape optimisation problems. It can also be applied to reduce the remeshing steps in the solution of coupled fluid-structure problems accounting for the movement of bodies.

The application of the different strategies to select the artificial Young modulus to be assigned to the pseudo-structural mesh elements shows that the geometric criteria are not effective if compared with the criteria based on structural parameters such as the strain field or the strain energy density.

Strategies based on the strain energy density, on the distortion energy density and on the square norm of the principle strains with a Poisson coefficient $\nu = 0.32$ showed the best results. The overall results obtained with the three strategies are very similar leaving to the programmer the choice of which one to implement.

Acknowledgements

This work has been supported by the EU Marie Curie Grant BRMA-CT97-5761 awarded to the first author. The authors want to acknowledge the support of E. N. BAZAN (Madrid) and of the International Centre of Numerical Methods in Engineering (CIMNE, Barcelona).

5. REFERENCES

[1] G. Chiandussi, G. Bugeda, E. Oñate "Shape variable definition with C^0, C^1 and C^2 continuity functions", Publication 134, CIMNE, 1998.

[2] O.C. Zienkiewicz, R.L. Taylor "The finite element method", McGraw Hill, 1989.

[3] M.H. Imam "Three dimensional shape optimisation", *International Journal for Numerical Methods in Engineering*, Vol. 18, pp. 661-673, 1982.

[4] V. Braibant, C. Fleury "An approximation-concepts approach to shape optimal design", *Computer Methods in Applied Mechanics and Engineering*, Vol. 53, pp. 119-148, 1985.

[5] V. Braibant, C. Fleury "Shape optimal design using B-splines", *Computer Methods in Applied Mechanics and Engineering*, Vol. 44, pp. 247-267, 1984.

[6] C. Farhat, "Parallel and distributed solution of coupled non linear dynamic aeroelastic response problems" in *Parallel Solution Methods in Computational Mechanics*. M. Papadrakakis (Ed.) J. Wiley, pp. 243-301, 1998.

[7] A. A. Johnson and T. B. Tezduyar, "Mesh update strategies in parallel finite element computations of flow problems with moving boundaries and interfaces". *Computer Methods in Applied Mechanics and Engineering*, Vol. 119, pp. 73-94, 1994.

[8] W. A. Wall and E. Ramm, "Fluid structure interaction based on a stabilized (ALE) finite element method" in *Computer Mechanics. New Trends and Applications*, S. Idelsohn, E. Oñate and E Dvorkin (Eds.). CIMNE, Barcelona, 1998.

[9] R. Löhner, C. Yang, E. Oñate and S. Idelsohn, "An unstructured grid based parallel free surface solver, 28th AIAA Fluid Dynamics Conference, June 29-July 2, 1997.

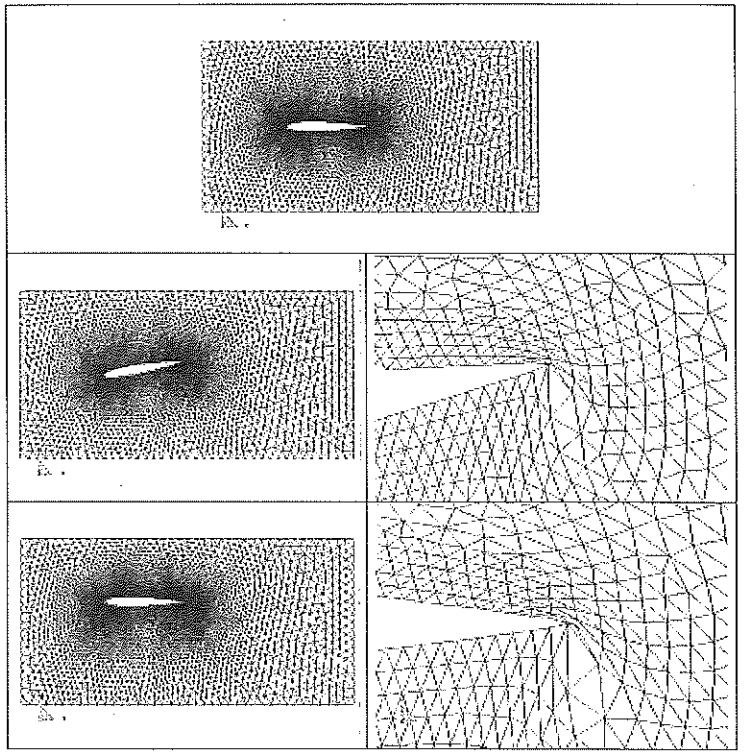

Figure 1: Original NACA0012 airfoil discrete model (first row). Tail vertical displacement and vertical change of position of the airfoil obtained for strategy 1 (general view and detail area with the most distorted elements). The maximum tail vertical displacement before element intersection has been about 18% of the chord length (second row). The maximum vertical displacement of the airfoil before element intersection has been about 24% of the chord length (third row). The 18% and the 24% chord length displacements for the two examples respectively will be used as a reference for the comparisons with results obtained with the other strategies.

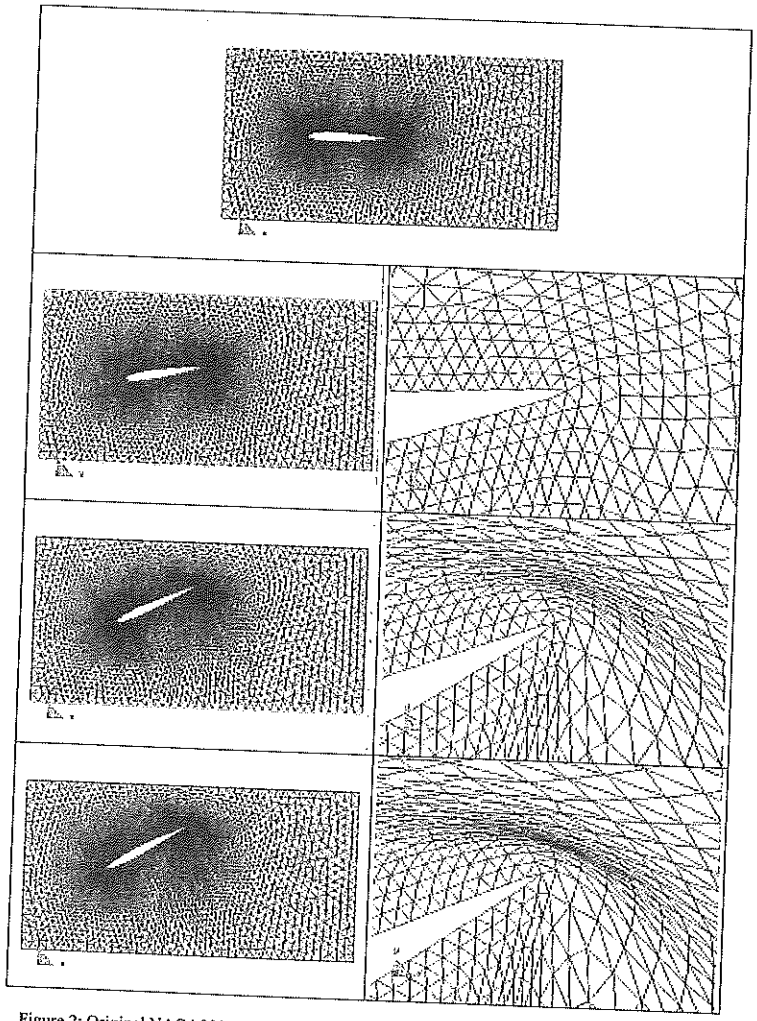

Figure 2: Original NACA0012 airfoil discrete model (first row). Tail vertical displacement of the airfoil using a Young modulus distribution depending quadratically on the distance from the elements to the moving surfaces (strategy 4). The 18% and the 50% chord length displacement are shown in the second and third row respectively. The maximum tail vertical displacement before element intersection has been about 55% of the chord length and is shown (fourth row).

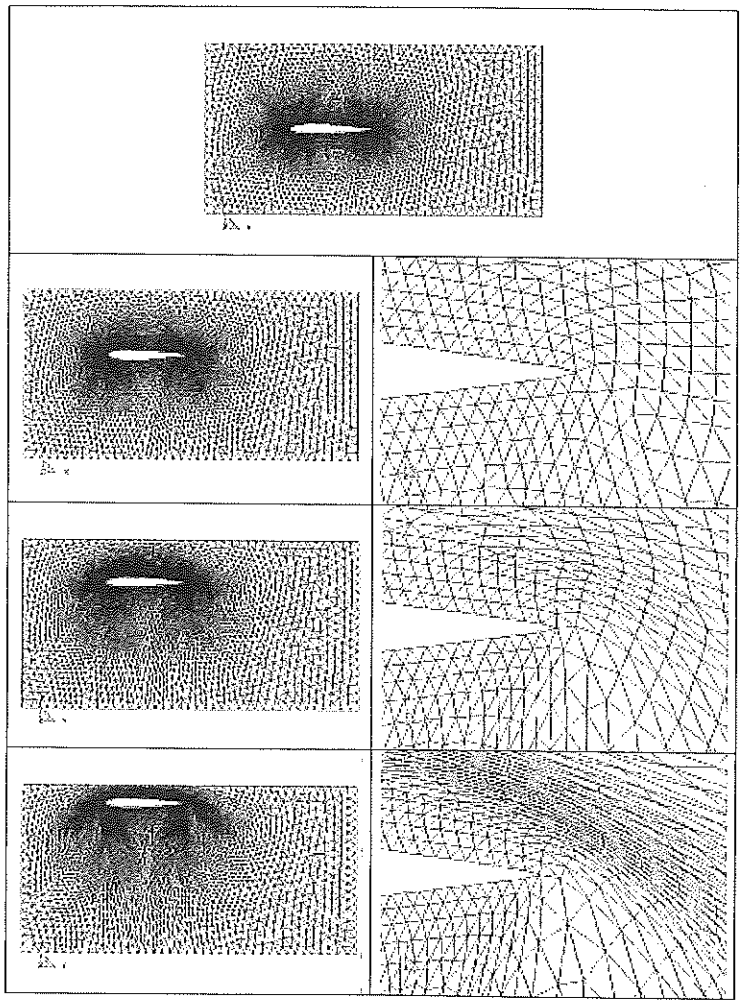

Figure 3: Original NACA0012 airfoil discrete model (first row). Vertical change of position of the airfoil using a Young modulus distribution depending quadratically on the distance of the elements from the moving surfaces (strategy 4). The 24% and 50% chord length displacement are shown in the second and third row respectively. The maximum vertical change of position before element intersection has been about 79% of the chord length (fourth row).

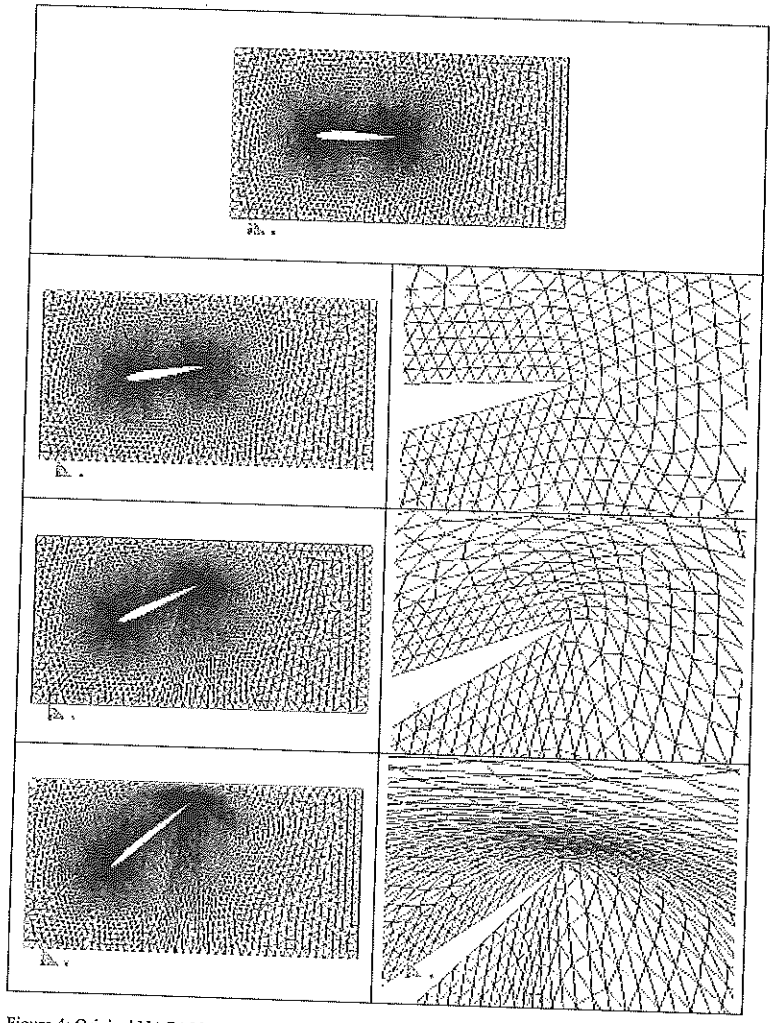

Figure 4: Original NACA0012 airfoil discrete model (first row). Tail vertical displacement of the airfoil using a Young modulus distribution depending on the strain energy density of the elements (strategy 6). The 18% and 50% chord length displacement are shown in the second and third row respectively. The maximum tail vertical displacement before element intersection has been about 84% of the chord length (fourth row).

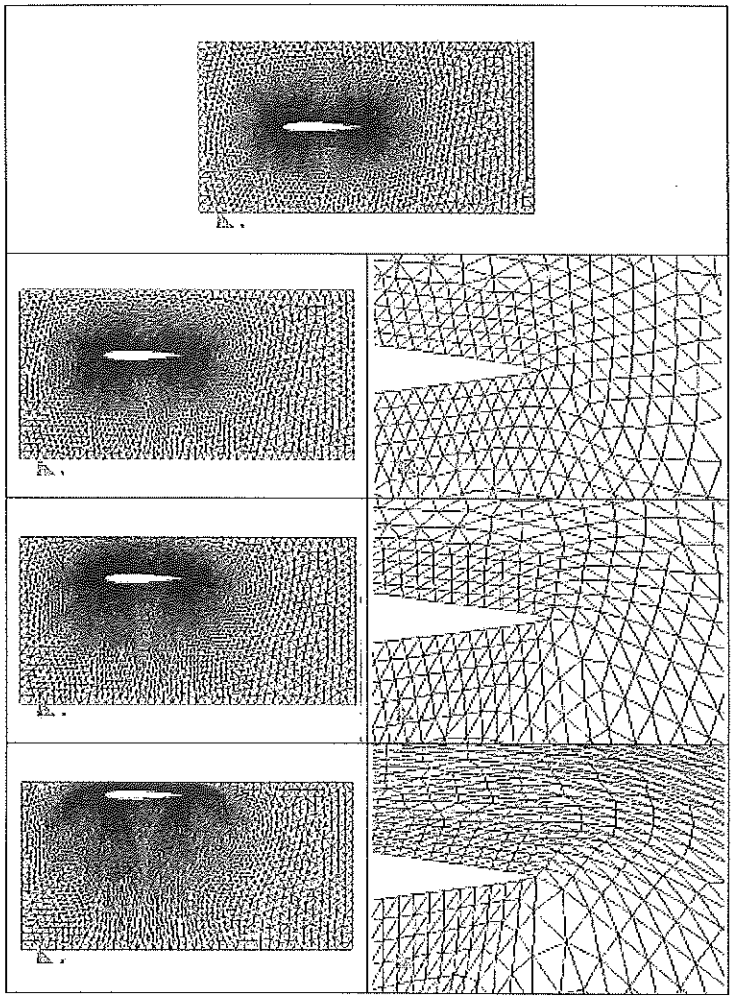

Figure 5: Original NACA0012 airfoil discrete model (first row). Vertical change of position of the airfoil using a Young modulus distribution depending on the strain energy density of the elements (strategy 6). The 24% and 50% chord length displacement are shown in the second and third row respectively. The maximum vertical change of position before element intersection has been about 85% of the chord length (fourth row).

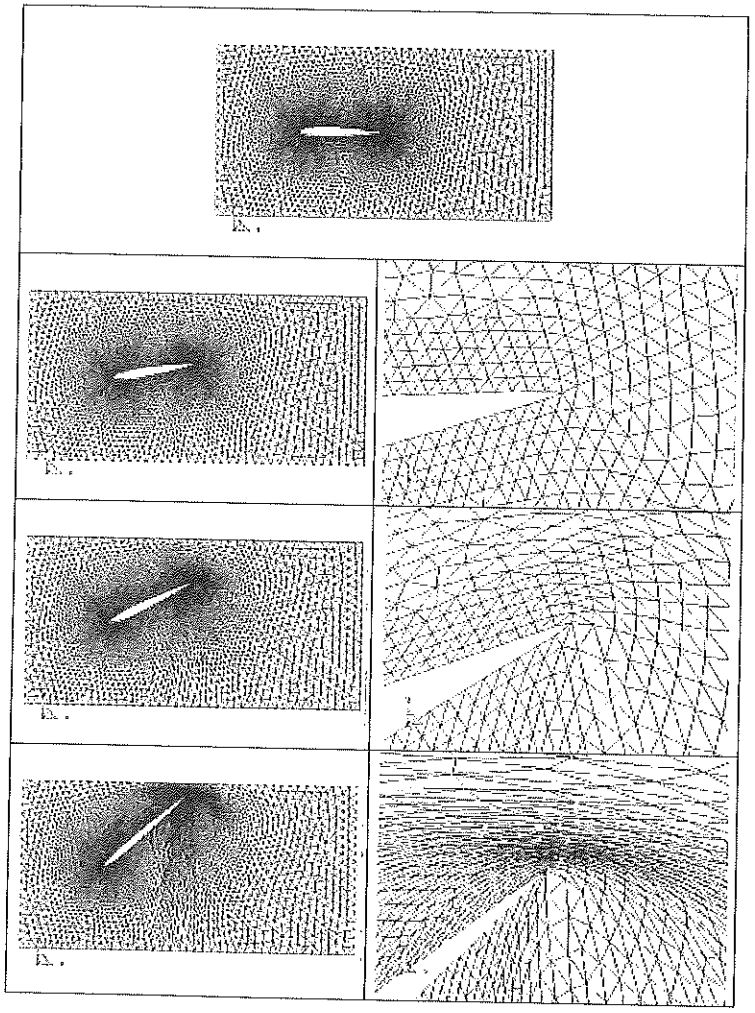

Figure 6: Original NACA0012 airfoil discrete model (first row). Tail vertical displacement of the airfoil using a Young modulus distribution proportional to the distortion energy density of the elements (strategy 7). The 18% and 50% chord length displacement are shown in the second and third row respectively. The maximum tail vertical displacement before element intersection has been about 82% of the chord length (fourth row).

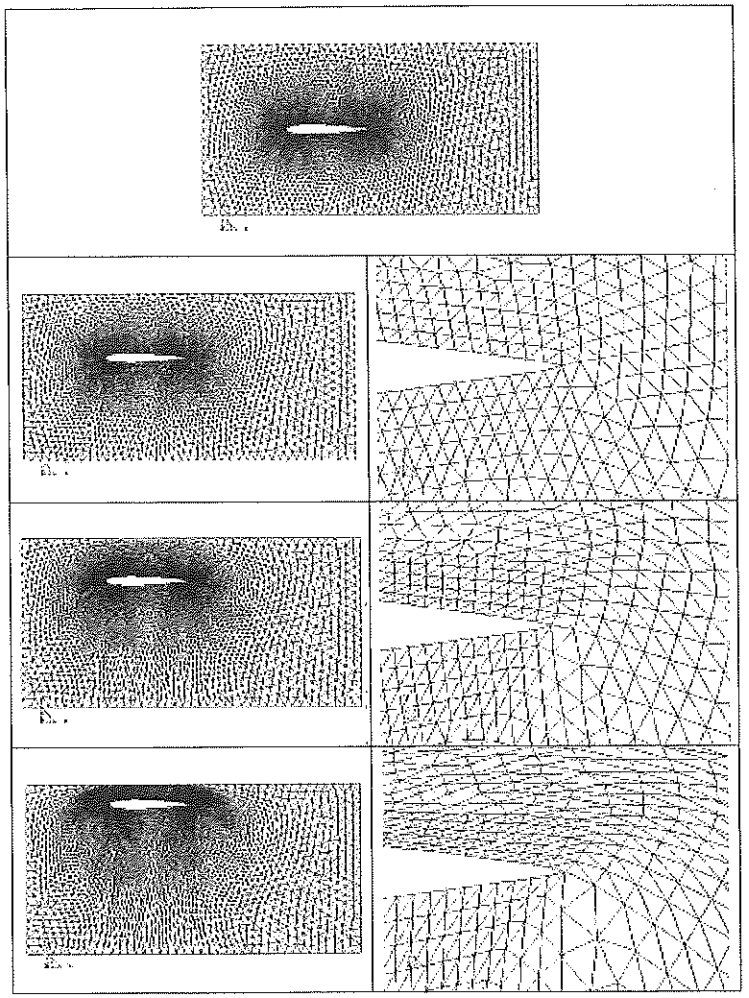

Figure 7: Original NACA0012 airfoil discrete model (first row). Vertical change of position of the airfoil using a Young modulus distribution proportional to the distortion energy density of the elements (strategy 7). The 24% and 50% chord length displacement are shown in the second and third row respectively. The maximum vertical change of position before element intersection has been about 80% of the chord length (fourth row).

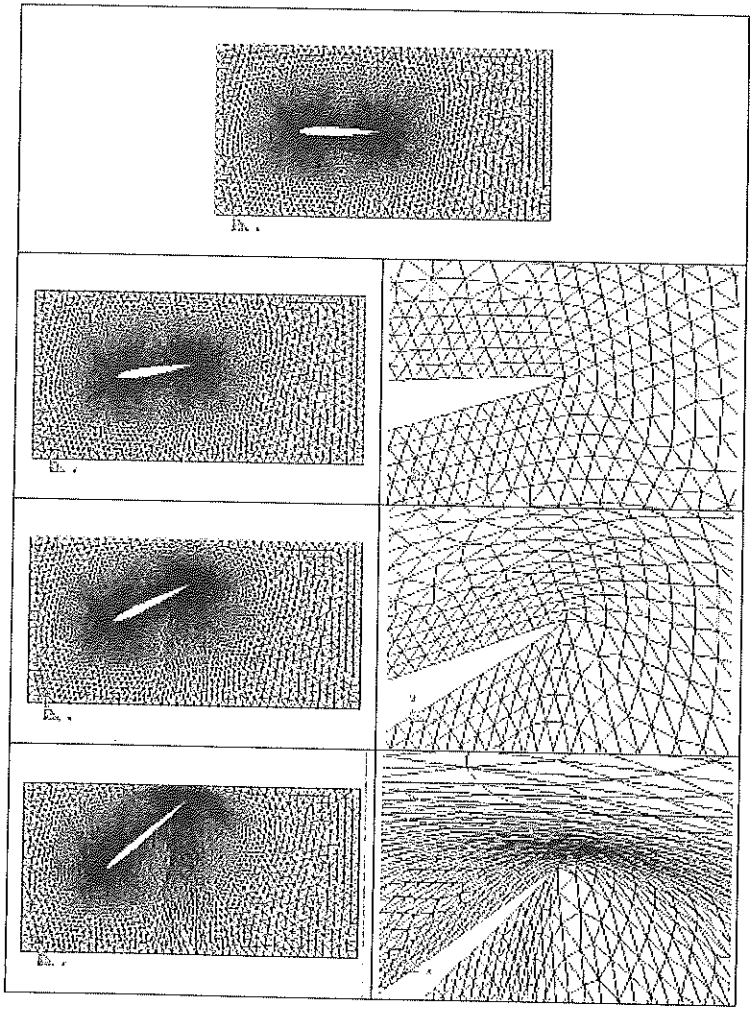

Figure 8: Original NACA0012 airfoil discrete model (first row). Tail vertical displacement of the airfoil using a Young modulus distribution depending on the square norm of the principal strains (strategy 8). The 18% and 50% chord length displacement are shown in the second and third row respectively. The maximum tail vertical displacement before element intersection has been about 87% of the chord length (fourth row).

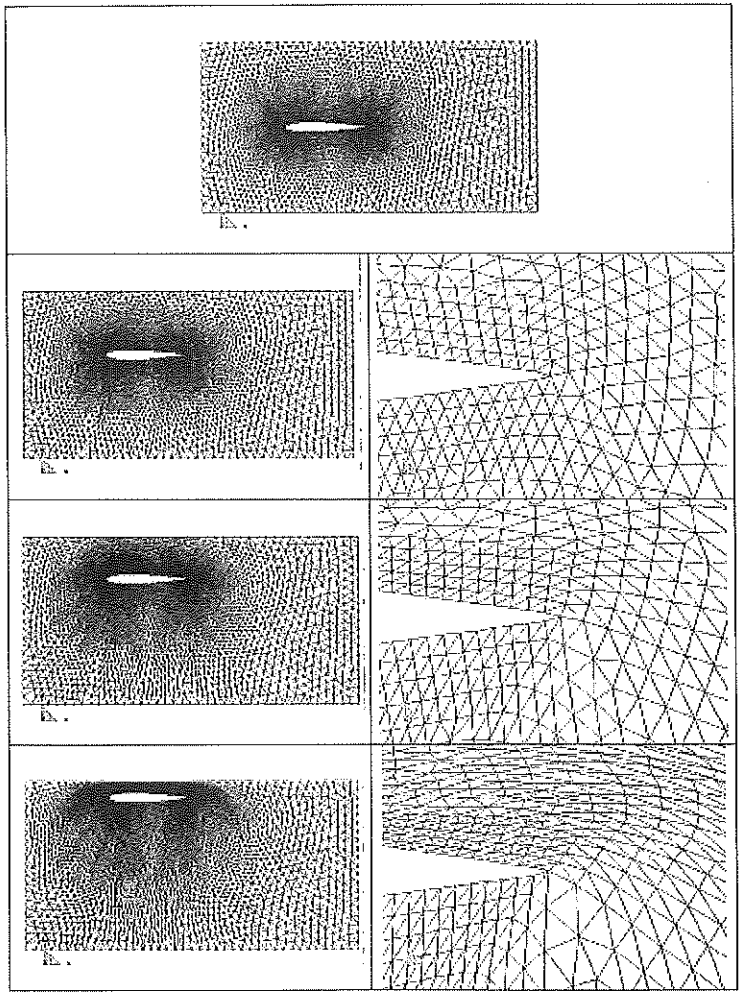

Figure 9: Original NACA0012 airfoil discrete model (first row). Vertical change of position of the airfoil using a Young modulus distribution depending on the square norm of the principal strains (strategy 8). The 24% and 50% chord length displacement is shown in the second and third row respectively. The maximum vertical change of position before element intersection has been about 81% of the chord length (fourth row).